Available online at www.sciencedirect.com
SCIENCE DIRECT®
Journal of Crystal Growth 265 (2004) 604–615
JOURNAL OF CRYSTAL GROWTH
www.elsevier.com/locate/jcrysgro

Nucleation and growth of crystalline ribbons in diastereomeric ephedrine–cyclic phosphoric acid systems

Joanne S.C. Loh, Willem J.P. van Enckevort*, Elias Vlieg

NSRIM Department of Solid State Chemistry, Faculty of Science, University of Nijmegen, Toernooiveld 1, 6525 ED Nijmegen, The Netherlands

Received 26 August 2003; accepted 12 February 2004
Communicated by D.T.J. Hurle

Abstract

In an attempt to understand the fast formation of diastereomerically enriched crystals in a Dutch resolution system, the nucleation and growth behaviour of such a system was investigated by in situ optical microscopy. Nucleation was observed to follow two pathways: nuclei crystal formation and ribbon formation. The shape of these ribbons (flat, helical or twisted) was dependent on the composition of the system. Hindrance during growth of the ribbons was observed to result in cleavage of the ribbons, creating new crystals. After continued growth, the ribbons develop into needles. This is most likely caused by the introduction of defects and not by a change in crystal polymorph.

PACS: 81.10.Aj; 81.10.Dn

Keywords: A1. Crystal morphology; A1. Nucleation; A1. Optical microscopy; A1. Ribbons; B1. Organic compounds

1. Introduction

The simultaneous use of more than one resolving agent from a 'family' of resolving agents is a new enantiomeric resolution technique called 'Dutch' resolution [1–3] (Scheme 1A). Similar to 'classical' resolution [4,5] (Scheme 1B), the resolving agents are chosen based on the nature of the racemate. For example, if the racemate is basic, an acidic resolving agent will be chosen, resulting in the formation of diastereomeric salts. Dutch resolution leads to improved resolution results as compared to 'classical' resolution, which proceeds by crystallization using a single resolving agent. The addition of more than one resolving agent results in rapid precipitation of crystalline diastereomeric salts in high yield and enantiomeric purity. There is also a high success rate in

$$R_BR'_B + A_1 + A_2 + A_3 \rightarrow R_BA_x + R'_BA_y\downarrow \quad (A)$$

$$R_BR'_B + A \rightarrow R_BA + R'_BA\downarrow \quad (B)$$

Scheme 1. 'Dutch' (A) and 'Classical' (B) resolution (R_B and R'_B are basic enantiomers, A_{1-3} are acidic resolving agents, R_BA_x and R_BA_y are resulting diastereomeric salt mixtures).

*Corresponding author. Tel.: +31-2436-53433; fax: +31-2436-53067.
E-mail address: wvenck@sci.kun.nl (W.J.P. van Enckevort).

0022-0248/$ - see front matter © 2004 Elsevier B.V. All rights reserved.
doi:10.1016/j.jcrysgro.2004.02.080

enantiomeric separation: only three out of 100 attempts were reported to have failed separation using this technique [1]. While the existing definition of a 'family' of resolving agents is not comprehensive, 'family' members generally share stereochemical homogeneity and strong structural similarities.

The observed fast formation of diastereomerically enriched salts, due to the addition of more than one member of a family of resolving agents, remains unexplained. The present research investigates the nucleation and growth behaviour using in situ optical microscopy of a model Dutch resolution system in an attempt to understand the increased crystallization rate. The model system consists of ephedrine (enantiomer of interest) and three members of the cyclic phosphoric acids family of resolving agents. This resolution system has been well-established [1,6,7].

2. Experimental procedure

The model system investigated comprises of the enantiomer of interest, (−)-ephedrine (**1**), and three (+)-members of the cyclic phosphoric acid 'family' of resolving agents; phencyphos, chlocyphos and anicyphos (**2–4**) (Table 1). The members of this family differ in the substitution on the aromatic ring. An ephedrine–cyclic phosphoric acid compound consists of a 1:1 mix of the two components to produce the compounds Inam (**5**), Clinam (**6**) and Aninam (**7**) (Table 1). The crystal structures of these compounds are known [8–10].

The (−)-ephedrine and cyclic phosphoric acid compounds were kindly donated by Syncom B.V. The cyclic phosphoric acids were synthesized and purified [6] while (−)-ephedrine was obtained from Sigma Chemicals (anhydrous, purity $\geqslant 98\%$).

The (−)-ephedrine-acid compounds were dissolved in ethanol on a hot plate at atmospheric pressure. The temperature was kept below the boiling point of the solution. Solutions were prepared to an initial supersaturation (β) of 1.5 or 2.0 (where $\beta = C_{\text{initial}}/C_{\text{equilibrium }25^\circ\text{C}}$) by weight. The solubility of the compounds in ethanol has been previously determined to be 9.5, 5.7 and 4.1 g per 100 g solution at 25°C for Inam, Clinam and Aninam, respectively [10]. For two-compound solutions, each compound had an individual initial supersaturation of 1.5 (we assumed there is no effect of compound B on the solubility of compound A and vice versa).

The solutions were filtered through a 0.2 μm syringe filter into a glass sample cell (2 ml), which was sealed with an airtight cap. The solutions were left unstirred. The sample cell was then placed into an experimental cell, which was connected to a temperature controlled water bath (similar to the set up described by Vogels et al. [11]). In this way strict control of the temperature ($\pm 0.2^\circ$C), and hence supersaturation, could be achieved. The

Table 1
The structures and nomenclature of (−)-ephedrine, (+)-cyclic phosphoric acids and the (−)-ephedrine-acid compounds

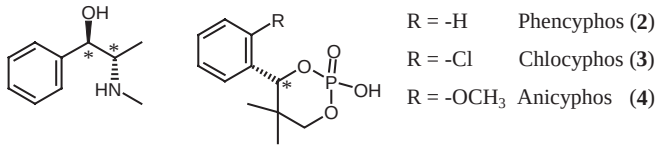

(-)-Ephedrine (**1**) (+)-Cyclic Phosphoric Acid

R group	(+)-Cyclic phosphoric acid (formal name)	(−)-Ephedrine-acid compound name	Space group of compound
–H	(+)-2-hydroxy-5,5-dimethyl-2-oxo-4-phenyl-1,3,2-dioxaphosphorinane (**2**)	Inam (**5**)	$P2_1$
–Cl	(+)-4-*o*-chlorophenyl-2-hydroxy-5,5-dimethyl-2-oxo-1,3,2-dioxaphosphorinane (**3**)	Clinam (**6**)	$P2_1$
$-OCH_3$	(+)-4-*o*-methoxyphenyl-2-hydroxy-5,5-dimethyl-2-oxo-1,3,2-dioxaphosphorinane (**4**)	Aninam (**7**)	$P2_12_12_1$

growing crystallites were visualized in situ using a Zeiss optical microscope (Axioplan2, transmission mode) at a magnification level of five. Digital images were captured using a CCD camera (Adimec, MX12P) and the software program ImagePro was used to handle the images. In a number of cases the crystals were also examined between crossed polarizers, which were mounted in the same microscope.

Increasing the temperature of the water bath could redissolve crystals that were formed in the sample cell during preparation. The temperature was then progressively decreased until nucleation commenced.

On various crystals single X-ray diffraction and powder X-ray diffraction was performed using a Nonius CAD4 diffractometer and a Philips PW1820 diffractometer using Cu Kα radiation ($\lambda = 1.54$ Å).

Crystals of two-compound solutions were also analysed by chiral high performance liquid chromatography (HPLC). An I.D. Chirobiotic R column (250×4.6 mm) was used to separate the enantiomers with a mixture of buffer/methanol (90:10 v/v %, where the buffer consisted of 15 mM ammonium acetate in water, pH 4.1). The flow rate used was 1 ml/min at a column temperature of approximately 21°C and an injection volume of 20 μl. A wavelength of 210 nm was used for detection.

3. Results

Nucleation and growth experiments were performed on one compound solutions as well as on mixtures of two compounds. Crystals were nucleated in all cases.

3.1. One-compound solutions

3.1.1. Inam (**5**)

Nucleation occurred relatively easily in Inam (**5**) solutions ($\beta = 1.5$). Elongated and blocky crystals formed (Figs. 1A and B, respectively). These two crystal types nucleated simultaneously and grew independently of each other. The structures of the two crystal types were determined to be the same by single crystal X-ray diffraction and are identical to that reported by Kok et al. [8]. Thus, the crystal shape differences were due to differences in the growth rates of the faces and not due to polymorphism.

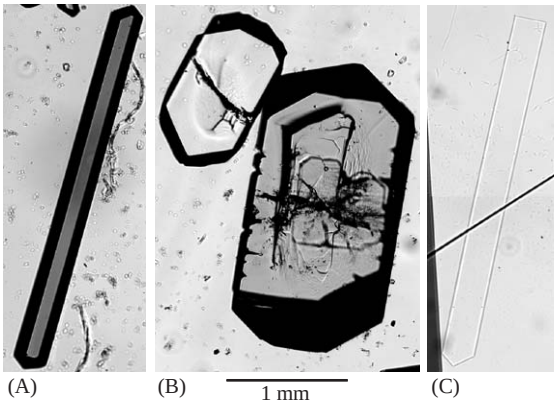

Fig. 1. Crystal shapes from a pure Inam (**5**) solution: (A) elongated, (B) blocky crystals and (C) ribbons.

Nucleation of Inam solution also produced 'ribbons' (Fig. 1C). The ribbons had well-formed and distinct straight edges, usually having an asymmetric form (as in the ribbon featured in Fig. 1C). This, as well as the observation of extinction in the polarization microscope if the longitudinal axis of the ribbons was parallel or perpendicular to the crossed polarizer directions, indicates that the ribbons are single crystalline. During growth of a ribbon its form was observed to change in a handful of cases, as depicted by the sequence of images in Fig. 2.

The ribbons were generally flat in orientation. These ribbons started very thin and increased in length, width and thickness, resulting in elongated crystals like the one shown in Fig. 1A (the increase in thickness can be observed through the changes in the opacity of the ribbon under optical microscopy). Growth of asymmetric ribbons produced asymmetric elongated needles. Symmetrical needles were also observed. Both types of needles were observed to also nucleate directly without originating from ribbons.

3.1.2. Clinam (**6**)

Nucleation only occurs in Clinam (**6**) solutions at an initial supersaturation (β) of at least 2. The

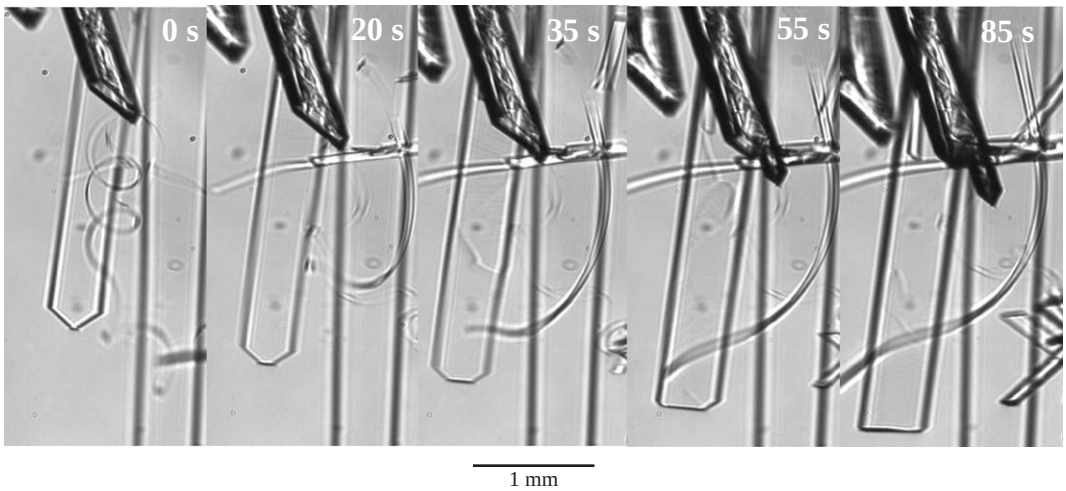

Fig. 2. Change in the shape of a ribbon end with growth from a pure Inam (**5**) solution.

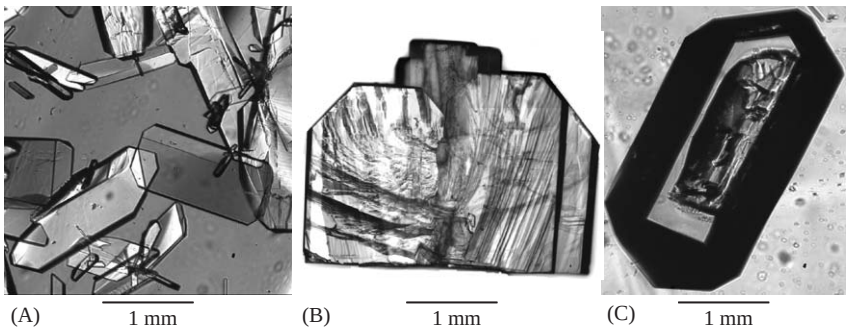

Fig. 3. Crystals from Clinam (**6**) (A and B) and Aninam (**7**) (C) solutions.

nuclei are thin (Fig. 3A) and 'mica'-like in their behaviour to agglomerate in layers (Fig. 3B). Once nucleation has occurred, growth is rapid. Powder XRD indicated that the crystals had the same crystal structure as that of the stable Clinam polymorph as reported by Smits et al. [9].

3.1.3. Aninam (**7**)

Nucleation only occurs in Aninam (**7**) solutions at an initial supersaturation (β) of at least 2. The nuclei and crystals are blocky in nature (Fig. 3C). Similar to Clinam, growth is rapid once nucleation has occurred. The structure of the crystals collected from these solutions was the same as the Aninam crystal structure determined by Gervais et al. [10].

3.2. Two-compound solutions

Each compound in the two compound solutions had an individual initial supersaturation of 1.5.

3.2.1. Inam with Clinam

Nucleation from an Inam–Clinam solution occurred relatively easily (nucleation occurred at 37°C, $\beta < 1.5$) and produced two types of nuclei, crystals and helical ribbons (Fig. 4A). The crystals and helical ribbons occurred simultaneously and grew independently of each other. The crystals

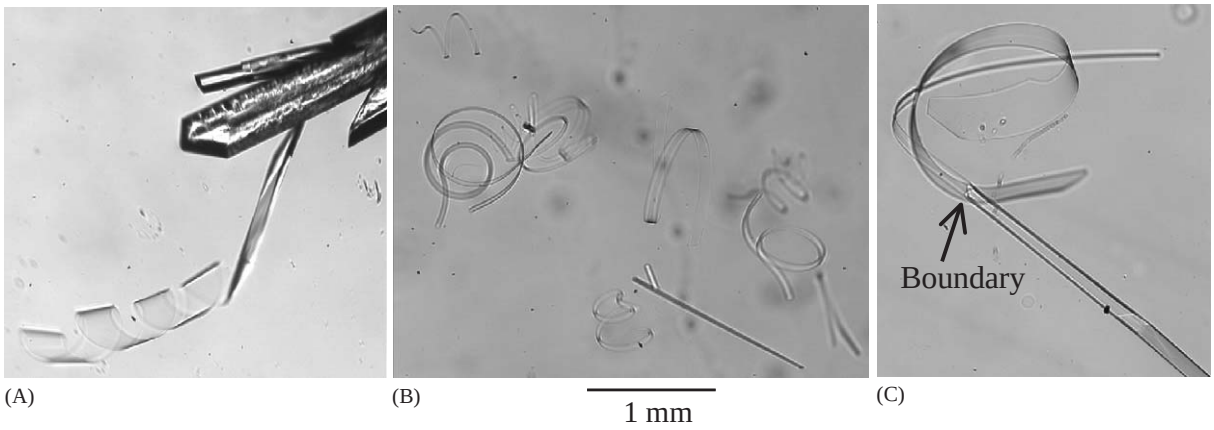

Fig. 4. Growth from Inam (**5**)/Clinam (**6**) two-compound solution: (A) crystals and wide helical ribbons, (B) thin helical ribbons and (C) a 'structure or thickness boundary' in a ribbon.

obtained from this mixture have an Inam crystal structure and consisted of a solid solution of Inam and Clinam at a ratio of 65:35 respectively (as determined from analysis of the X-ray diffraction data). Inam and Clinam are distributed throughout the crystal in a random manner. This result is consistent with the observed solubility behaviour of this system [10].

The helical ribbons can be either flat and wide, or very thin, like filaments (Fig. 4B) and usually occurred with a similar asymmetric shape as the ribbons produced in pure Inam solutions (Fig. 1C). Both left- and right-handed helices were found to grow in the same solution. Growth of the helical ribbons progressed with increases in length, width and thickness, resulting in elongated needle crystals similar in shape to those observed in pure Inam solution (Fig. 1A). There was 'orderly' growth of the ribbons, generally starting at one end of the ribbon, increasing in thickness along the length of the ribbon (this is observable through the changes in opacity of the ribbon by optical microscopy, as well as by an increase in intensity between crossed polarizers with the crystal in the 45° position). In a few cases a 'boundary' was observed in a ribbon, separating areas of ribbon flexibility and more crystalline rigidness (Fig. 4C). This 'boundary' was observed to move along the length of the ribbon as growth progressed.

The growth of a helical ribbon from both ends was also observed. Growth occurred first at End 1 (Fig. 5A) with the disordered formation of elongated crystals as well as the thickness growth and straightening out of the ribbon itself (note the difference in opacity). After 1 min, both Ends 1 and 2 (Fig. 5B) are growing. However, the growth behaviour of the two ends is different. The thickness of the ribbon of End 2 does not seem to increase as indicated by an absence of a difference in the opacity of the ribbon. End 2 grows and elongates, straightening out as it grows (Fig. 5C) without significant thickening of the ribbon or a clear 'growth zone'. The orderly growth of End 1 produced a wedge-shaped profile. There is no opportunity for the ribbon to unwind as End 2 grows.

The tension in the ribbon increases as End 2 grows (Fig. 5D) until it breaks or cleaves (Fig. 5E), resulting in two separate crystals. The ribbon is now free to unwind at the new ribbon end, End 3 (Fig. 5F). End 3 begins to grow with increasing thickness, in a similar manner to the growth behaviour of End 1, straightening out the ribbon in the process. The remaining portion of the flexible ribbon then cleaves again (approximately 90 s later) as Ends 1 and 3 grow towards one another. As a result, a total of three separate crystals were produced from one helical ribbon.

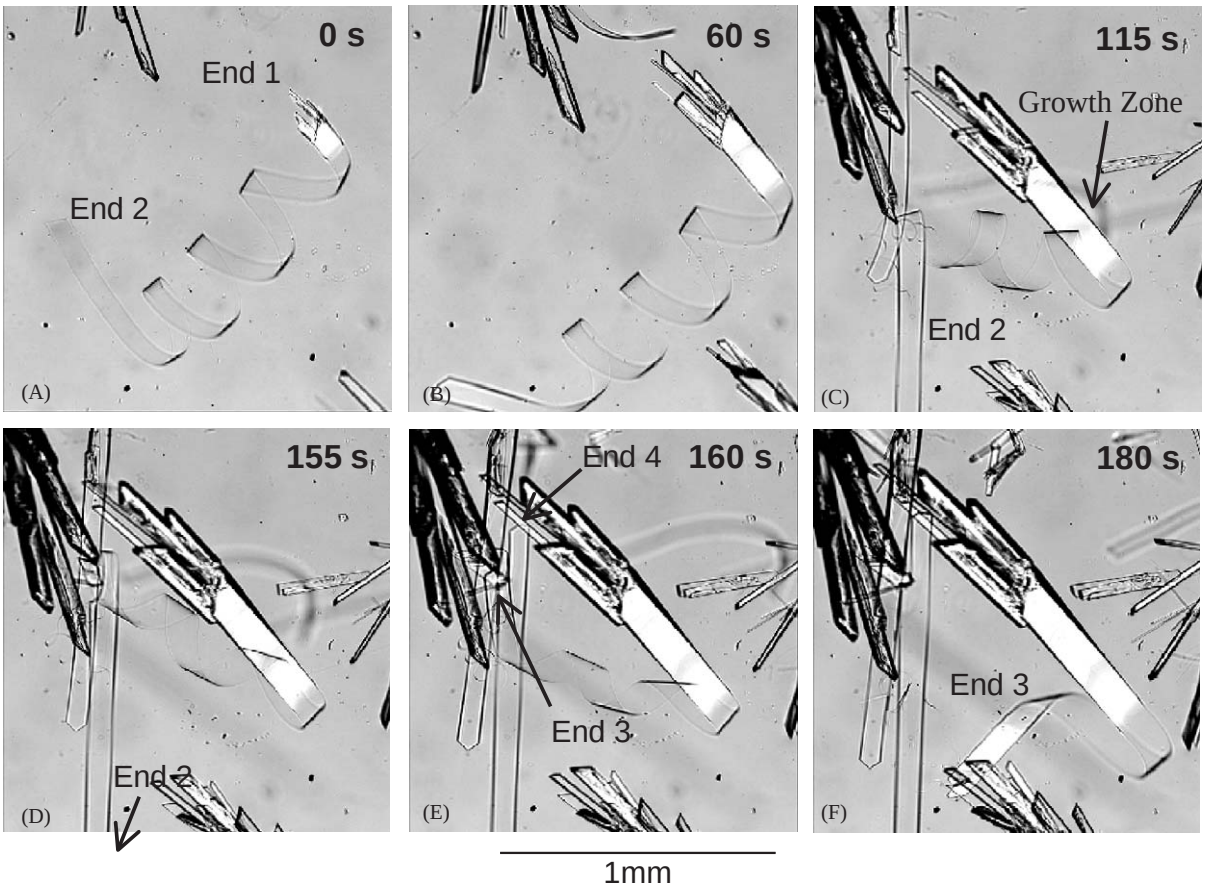

Fig. 5. A sequence of photos showing the growth of a helical ribbon with time.

3.2.2. Inam with Aninam

Nucleation readily occurred in an Inam–Aninam solution (nucleation occurred at 25°C, $\beta = 1.5$). Very thin and flexible needles were produced existing as agglomerates predominantly joined at one point (Fig. 6A). With growth, the needles grew only slightly in thickness and thin, crystalline needles were produced. The powder XRD pattern indicated that the crystals obtained from this solution had the Inam crystal structure. This is inconsistent with the expected product as predicted from the solubility phase diagram [10]. This system is eutectic in nature and Aninam is the predicted product from the initial solution composition used in the present work (50% Inam and 50% Aninam). However, due to the fact that the experimentally derived product is not obtained under thermodynamic equilibrium conditions, kinetic factors may have affected the composition of the final product.

Crystals produced under similar conditions consisted mainly of Inam with approximately 1.3% Aninam (as determined by HPLC). The observation of a small amount of Aninam might be due to an increased limit of detection in the HPLC method currently used in comparison to the method used in Gervais et al. [10]. Alternatively part of an Aninam crystal was also present in the sample that was analysed.

Thin, flexible ribbons were also observed (Fig. 6B). These ribbons only constituted less than 5% of the crystals formed in this solution. These

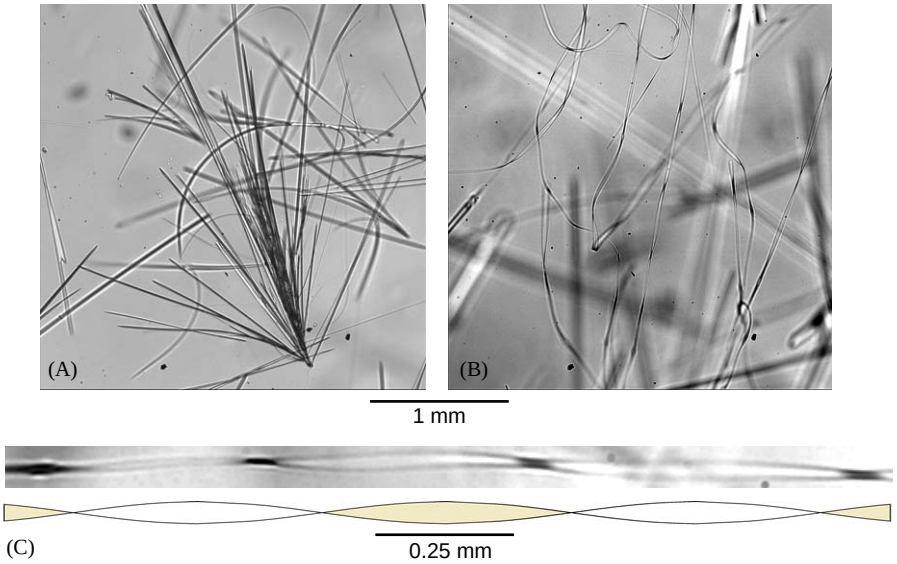

Fig. 6. Nuclei forms from Inam/Aninam two-compound solution, (A) thin needles, (B) twisted ribbons, (C) a close up of a twisted ribbon and a schematic representation of a twisted ribbon.

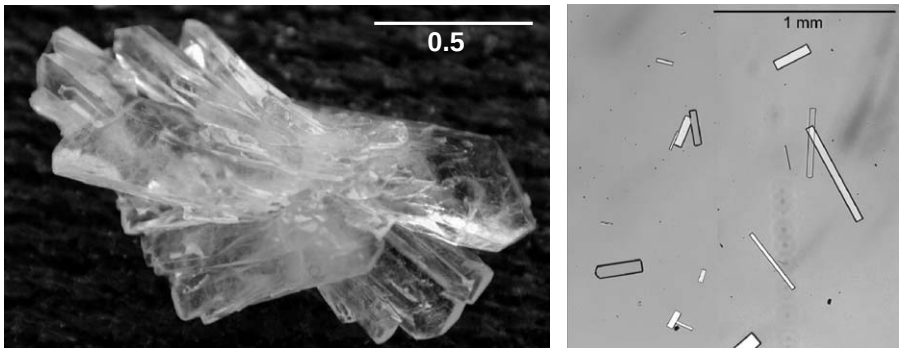

Fig. 7. Nuclei from Clinam/Aninam two-compound solution consist of elongated crystals.

ribbons were twisted in a tighter fashion than the helical ribbons (compare Fig. 5A with Fig. 6C). With growth the flexible ribbons developed into thin, crystalline needles.

3.2.3. *Clinam with Aninam*

Two types of crystals formed from a Clinam–Aninam solution ($\beta = 1.5$ for each compound). An agglomerate of elongated crystals was initially formed prior to the nucleation of isolated elongated crystals (Figs. 7A and B). While several flat rectangular ribbons were observed, the large majority (99%) of the nuclei was crystals. The elongated crystals consisted of a solid solution of Clinam and Aninam (in the ratio of 75:25, respectively, as determined from analysis of X-ray diffraction data) in an Aninam crystal structure. The observed crystal structure and ratio of the compounds are consistent with the solid solution behaviour determined from the solubility

phase diagram of this system [10]. Helical or twisted ribbon formation was not observed in the Clinam–Aninam solution.

4. Discussion

4.1. Crystals and ribbons

Our observations are summarized in Scheme 2. Two crystallization pathways have been observed in the present system. Crystals and ribbons were observed simultaneously and once formed, grew independently of each other. The different morphologies of the crystals—blocky or elongated—were a result of differences in the growth rate of the crystal faces and not due to polymorphism.

Four different types of single crystal *ribbons* were observed; filament, flat, helical and twisted ribbons. Helical or twisted ribbons were only observed in two-compound solutions. All types of ribbons grew with increases in thickness, width and length, producing elongated crystals.

While nucleation in the pure solutions of Clinam and Aninam was quite difficult, we found that nucleation from mixtures was always easy. This confirms the enhanced nucleation generally observed in Dutch Resolution systems. An explanation cannot readily be given. Possibly the second compound covers (partly) the surfaces of the 3D germs, thereby lowering their surface free energy. This again reduces the barrier for supercritical nucleus formation. It is interesting to note that also the inhibition of nucleation plays a key role in a Dutch resolution system, by suppressing the crystallization of the undesired diasteriomeric salts [12].

4.2. Ribbons

4.2.1. Origin

The appearance of ribbons in our model system was surprising and unexpected. The formation of ribbons, both flat and helical, has been widely reported in amphiphilic molecules, a group of molecules which contains both hydrophilic and hydrophobic regions [13]. While the present compounds possess these regions, our ribbons have an average thickness between 1 and 10 μm (measured after some growth of the ribbon had taken place) and are, therefore, many hundreds of layers thick. Thus, the bilayer theory, used to explain ribbon formation of the amphiphilic molecules, is not applicable to our system.

To the best of our knowledge, this is the first time ribbon formation has been reported for these types of solutions. Ribbon formation was not

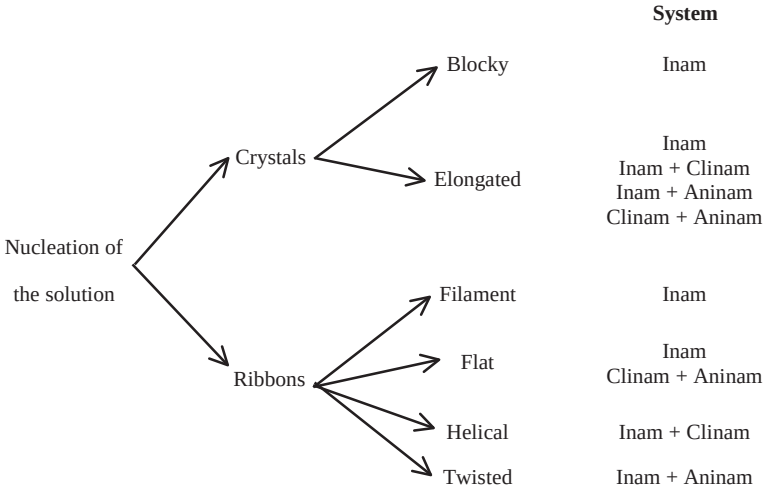

Scheme 2. Possible growth pathways observed for the present solutions. After continued growth, the ribbons develop into elongated needles.

observed in the nucleation of solutions of individual components (−)-ephedrine (**1**), (+)-phencyphos (**2**), (+)-chlocyphos (**3**) or (+)-anicyphos (**4**) at similar concentrations in ethanol. Thus, ribbon formation is exclusively due to the interaction between (−)-ephedrine and cyclic phosphoric acid.

There are two possible explanations for the origin of the ribbons in the present system: firstly, the ribbons could be a metastable polymorph which transforms into the stable polymorph, or, secondly, the ribbons could have the same crystal structure as the final products, but acquire the ribbon morphology due to the growth kinetics. These two hypotheses will be discussed in relation to the simultaneous existence of thin and thick ribbons and flat and helical ribbons.

4.2.2. Ribbons—thin versus thick

The ribbons observed in the current system could initially exist as a polymorph with such a crystal structure that the growth morphology is very anisotropic. This polymorph goes through a solid state transformation to the final (stable) product that has a more compact growth morphology. A first-order solid state transition commonly introduces a structure boundary as observed in Figs. 4C and 5. For this type of phase transition the boundary between the two domains is abrupt and will move along the ribbon with time. The observed thickening is then explained by a faster growth of the planar side faces of the stable polymorph. This leads to the development of crystal needles, like the one shown in Fig. 1A. The boundary between the two phases is observed to be "coherent": a single crystal ribbon turns into a single crystal needle with the same orientation and without the introduction of visible defects. In addition, the projected angles of the end faces on the upper and lower {1 0 0} faces do not change during transformation. These observations indicate that the crystal structure of our hypothetical polymorph must be very close to that of the stable phase, for all systems investigated. Thus polymorphism is less likely to explain the origin and growth of the ribbons in the present system.

The second explanation assumes that the ribbons have the same crystal structure as the final product. The different growth morphologies then originate from differences in defect densities. After initial nucleation, a number of the crystallites could be free from dislocations, meaning that they can only grow by a 2D nucleation mechanism. Then, the growth rate of each face ($h\,k\,l$) is strongly dependent on its step free energy, $\gamma_{\mathrm{st},hkl}$, according to

$$R_{hkl} \propto \exp\left(-\frac{\pi\gamma_{\mathrm{st},hkl}^2 s}{3\Delta\mu kT}\right), \tag{1}$$

where $\Delta\mu/kT$ is the dimensionless driving force for growth, k is the Boltzmann constant, T is the temperature and s is the surface area per growth unit. This implies that differences in $\gamma_{\mathrm{st},hkl}$ for the different faces of a crystal lead to a morphology with a very large aspect ratio. For perfect Inam crystals, 2D nucleation growth would cause the {1 0 0} faces to grow extremely slowly as compared to the other faces of the crystal and very thin ribbons are formed. A similar, even more extreme case is the growth form of a perfect $C_{40}H_{82}$ *n*-paraffin crystal from solution, which was proved to be a platelet of monomolecular thickness [14]. For Inam crystals containing dislocations, growth proceeds by the spiral mechanism, where the step density and, crudely, the growth rate is inversely proportional to $\gamma_{\mathrm{st},hkl}$. This reduces the differences in growth rate of the different faces, leading to block or needle-shaped crystals.

In this picture, the gradual thickening of the Inam ribbons is due to the introduction of dislocations at the end of the ribbons leading to spiral growth. Spiral growth produces an unlimited supply of steps on the surface of the ribbon, resulting in a wedge-shaped profile as growth proceeds. This wedge-shaped profile is nearly always observed when a ribbon transforms into a needle. In a few cases, a macrostep may develop leading to an abrupt change in thickness, which is visible as a "boundary", like the one shown in Fig. 5C. Since no phase transformation occurs during spiral growth, it is obvious that the projected angles of the end faces on the upper and lower {1 0 0} faces will not change during the conversion of the ribbons. Also the 'coherency' of the transformation is readily explained.

Spiral growth may be observed in the sequence of photos in Fig. 5. Dislocations are present in End 1 (Fig. 5A) where elongated needles are growing from the end of the ribbon. There is a boundary (difference in the opacity of the ribbon) present which proceeds along the ribbon with growth. This boundary is the border between the original ribbon thickness and the first spiral steps. The ribbon-crystal increased in thickness to form a wedge-shaped crystal. Thus spiral growth explains the observations at End 1.

Growth at End 2 occurred through a different mechanism. No boundary was observed and there was no obvious thickening of the ribbon. Growth progressed through the lengthening of the ribbon by fast 2D nucleation on the top faces with no significant increases in width or thickness. Only when End 2 had cleaved to produce End 3 (Fig. 5E) did the ribbon increase in thickness and a boundary was observed. Cleavage of the ribbon is likely to have introduced dislocations in the ribbon and spiral growth becomes the mechanism through which the ribbon then grew. Spiral growth steps are commonly observed on the Inam crystals as shown in Fig. 8.

The proposed mechanism of thin and thick ribbon formation is also consistent with the preferred formation of ribbons in Inam-containing solutions at lower supersaturations (i.e. at higher temperatures). At such supersaturations, it is more likely that defect-free crystals are formed. High supersaturations promote defect formation which leads to spiral growth and thicker ribbons and crystals.

An additional argument comes from thermodynamics. It is well known that a crystal of a metastable polymorph in a solution containing crystals of the stable phase at not too high supersaturation is expected to dissolve. However, we never observed dissolving ribbons in the neighbourhood of a needle or block shaped crystal, even if the supersaturation was low. This fact and Ockham's razor (the simplest explanation is the best) favours the spiral growth hypothesis. Unfortunately the ribbons are too flexible, too thin and too short-lived to allow structure determination using X-ray diffraction or Raman spectroscopy.

4.2.3. *Ribbons—flat versus helical/twisted*

Flat and twisted/helical ribbons were observed in the present system. The most generally accepted explanation for twisted and helical ribbons (and tubules) formation of amphiphilic molecules is based on the tilted packing order of these chiral molecules. While the molecules in the present system are chiral, molecular chirality may not be an essential factor in ribbon formation. Achiral 2,4,6-trichlorophenol has been observed to form long flexible filaments, sheets, helical and twisted ribbons and tubules in water [15]. But also for this case, bilayers are formed [16]. No bilayers occur for the present diastereomeric salts, so a different mechanism must be active here.

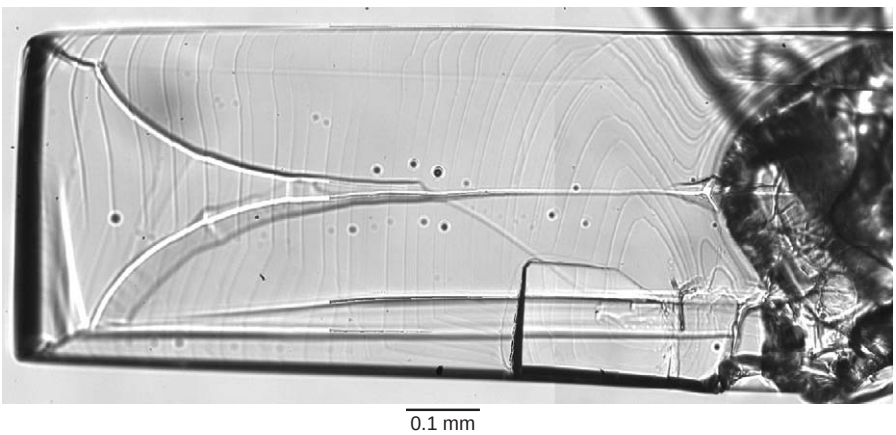

Fig. 8. Step formation on an Inam crystal.

In pure Inam solutions, only filaments or flat ribbons are observed. Twisted or helical ribbons are exclusively observed in Inam mixtures. This suggests that the additional presence of Aninam or Clinam in an Inam solution induces or promotes twist or helical formation in the ribbons. Here the incorporation of the second component into the Inam crystal structure causes the deformation of the ribbons. The final product from these mixtures crystallizes in the Inam space group $P2_1$, i.e. point group 2 (Fig. 9).

The twisted ribbons, only observed in the Inam–Aninam solution, are consistent with point group 2, i.e. the opposite {1 0 0} sides of the twisted ribbons are symmetrically equivalent. A small amount of Aninam was detected, thus Aninam can, to a small extent, incorporate in the Inam crystal structure. Indeed, the Aninam ($P2_12_12_1$) and Inam ($P2_1$) unit cells possess a two-dimensional slice in common. The addition of an Aninam unit cell into an Inam crystal structure may result in a small rotation along the *b*-axis. A rotation of only 3×10^{-4} degrees per unit cell length is required for the observed twisting to occur.

Helical ribbons are only observed in the Inam–Clinam solution. However, the helical ribbons are not consistent with point group 2 symmetry and instead, possess a point group symmetry for which the opposite faces (1 0 0) and ($\bar{1}$ 0 0) are not equivalent. The incorporation of Clinam is different for the opposite (1 0 0) growth sectors and thus leads to symmetry breaking. We do not have a definitive explanation for this, but maybe in this case the ribbons are a metastable polymorph. Note that the symmetry breaking is very small and is not easily detected using X-ray diffraction. The simultaneous presence of left- and right-handed helices in the growth solution suggests that chirality of the compounds involved is not essential in helix formation.

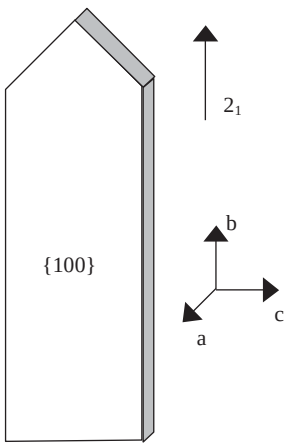

Fig. 9. Morphology of a flat Inam ribbon.

After transformation, the two opposite {1 0 0} faces become symmetrically equivalent and impurity segregation in the associated growth sectors gets identical. Moreover, the crystal thickens quickly and flexibility is readily lost. From strength theory it is known that the bending resistance of a free elastic beam increases with the third power of its thickness [17]. So, the ribbons straighten out and turn into needles. Helices and filaments as an intermediate state prior to the development of thicker crystal plates were also found for cholesterol crystallising from a bile salt-rich model bile [18].

The application of spiral growth theory to the growth of ribbons does not explain the curving of the ribbons when growth takes place in the Inam–Clinam solution. As previously stated, in the point group 2 of Inam the two opposing faces (1 0 0) and ($\bar{1}$ 0 0) are symmetrically equivalent and impurity incorporation in the associated growth sectors should be theoretically identical. No bending should occur. Therefore, the helix formation of the ribbons is introduced by another, unknown, mechanism or the morphological symmetry of Inam is lower than the symmetry as determined by X-ray diffraction. Such a decrease in morphological symmetry is a phenomenon called hypomorphism [19,20] and has been observed in $NH_4H_2PO_4$ [21], $K_2Cr_2O_7$ [22,23], and gibbsite, $Al(OH)_3$ [24].

5. Conclusions

The nucleation behaviour of an ephedrine–cyclic phosphoric acid model system has been investigated. The addition of more than one cyclic phosphoric acid significantly changes the interactions between (−)-ephedrine and cyclic phosphoric acid. Faster nucleation rates from two compound

mixtures relative to the individual compound solutions were observed, in agreement with the enhanced nucleation generally observed in Dutch Resolution systems. Nucleation of Inam-containing solutions proceeds through two pathways, namely through the formation of crystals and ribbons. The addition of Clinam promotes the formation of helical ribbons, while the presence of Aninam produces twisted ribbons. Under certain conditions, helical ribbons cleave or break, producing new crystals. This again enhances nucleation in Dutch resolution as compared with the classical resolution method for enantiomeric separation.

The transformation of ribbons to needles is most likely caused by the introduction of defects, leading to a transition from 2D nucleation growth to spiral growth. An alternative explanation involving a metastable polymorph is less likely. The formation mechanism and nature of helical curving of the ribbons in the Inam-Clinam solutions remains unknown.

Acknowledgements

The authors would like to thank L. Duchateau (DSM Research, Geleen) for HPLC analyses and Dr. R. de Gelder for X-ray diffraction work. Further they are grateful to Dr. H. Meekes (University of Nijmegen) for stimulating discussions and to Dr. B. Kaptein (DSM Research, Geleen) for critically reading the manuscript. The authors would like to acknowledge DSM and the Netherlands Organization for Scientific Research (STW-NWO) for financial support.

References

[1] T. Vries, H. Wynberg, E. van Echten, J. Koek, W. ten Hoeve, R.M. Kellogg, Q.B. Broxterman, A. Minnaard, B. Kaptein, S. van der Sluis, L. Hulshof, J. Kooistra, Angew. Chem. Int. Ed. 37 (1998) 2349.
[2] Q.B. Broxterman, E. van Echten, L.A. Hulshof, B. Kaptein, R.M. Kellogg, A.J. Minnaard, T.R. Vries, H. Wynberg, Chimica Oggi (Chem. Today) 16 (1998) 34.
[3] B. Kaptein, H. Elsenberg, R.F.P. Grimbergen, Q.B. Broxterman, L. Hulshof, K.L. Pouwer, T.R. Vries, Tetrahedron: Asymmetry 11 (2000) 1343.
[4] L. Pasteur, Ann. Chim. Phys. 24 (1848) 442.
[5] L. Pasteur, C.R. Hebd, Seances Acad. Sci. 37 (1853) 162.
[6] W. ten Hoeve, H. Wynberg, J. Org. Chem. 50 (1985) 4508.
[7] F.J.J. Leusen, J.H. Noordik, H.R. Karfunkel, Tetrahedron 49 (1993) 5377 (and references herein).
[8] A.M.G. Kok, H. Wynberg, J.M.M. Smits, P.T. Beurskens, V. Parthasarathi, Acta. Cryst. C 43 (1987) 1328.
[9] J.M.M. Smits, P.T. Beurskens, V. Parthasarathi, E.A. Rijk, A.M.G. Kok, H. Wynberg, Acta. Cryst. C 43 (1987) 1334.
[10] C. Gervais, R.F.P. Grimbergen, G.J.A. Ariaans, B. Kaptein, A. Bruggink, Q.B. Broxterman, J. Am. Chem. Soc. 126 (2004) 655.
[11] L. Vogels, H. Marsman, M. Verheijen, J. Crystal Growth 100 (1990) 439.
[12] J.W. Nieuwenhuijzen, R.F.P. Grimbergen, C. Koopman, R.M. Kellogg, T.R. Vries, K. Pouwer, E. van Echten, B. Kaptein, L.A. Hulshof, Q.B. Broxterman, Angew. Chem. 114 (2002) 22.
[13] V.S. Kulkarni, J.M. Boggs, R.E. Brown, Biophys. J. 77 (1999) 319.
[14] M. Plomp, W.J.P. van Enckevort, P.J.C.M. van Hoof, C.J. van de Streek, J. Crystal Growth 249 (2003) 600.
[15] E. Rogalska, M. Rogalski, T. Gulik-Krzywicki, A. Gulik, C. Chipot, Proc. Natl. Acad. Sci. USA 96 (1999) 6577.
[16] C. Chipot, J. Phys. Chem. B 105 (2001) 5987.
[17] J.P. Den Hartog, Strength of Materials, Dover Publications Inc., New York, 1949.
[18] F.M. Konikoff, D.E. Cohen, M.C. Carey, J. Lipid Res. 35 (1994) 60.
[19] A. Shubnikov, Z. Krist. 40 (1911) 19.
[20] A. Shubnikov, Z. Krist. 76 (1931) 469.
[21] M.A. Verheijen, L.J.P. Vogels, H. Meekes, J. Crystal Growth 160 (1996) 337.
[22] M. Plomp, A.J. Nijdam, W.J.P. van Enckevort, J. Crystal Growth 193 (1998) 389.
[23] M. Plomp, W.J.P. van Enckevort, E. Vlieg, J. Crystal Growth 216 (2000) 413.
[24] C. Sweegers, M. Plomp, H.C. de Coninck, H. Meekes, W.J.P. van Enckevort, I.D.K. Hiralal, A. Rijkboer, Appl. Surf. Sci. 187 (2002) 1.